



Editor's Pick | Virology | Full-Length Text

Mouse hepatitis virus JHMV I protein is required for maximal virulence

Shea A. Lowery,¹ Noah Schuster,¹ Lok-Yin Roy Wong,¹ Thomas Carrillo Jr.,¹ Erin Peters,¹ Abby Odle,¹ Alan Sariol,¹ Isabella Cesarz,¹ Pengfei Li,¹ Stanley Perlman^{1,2}

AUTHOR AFFILIATIONS See affiliation list on p. 21.

ABSTRACT Betacoronaviruses encode a conserved accessory gene within the +1 open reading frame (ORF) of nucleocapsid called the internal N gene. This gene is referred to as "I" for mouse hepatitis virus (MHV), ORF9b for severe acute respiratory CoV (SARS-CoV) and SARS-CoV-2, and ORF8b for Middle East respiratory syndrome CoV (MERS-CoV). Previous studies have shown ORF8b and ORF9b have immunoevasive properties, while the only known information for MHV I is its localization within the virion of the hepatotropic/neurotropic A59 strain of MHV. Whether MHV I is an innate immune antagonist or has other functions has not been evaluated. In this report, we show that the I protein of the neurotropic JHM strain of MHV (JHMV) lacks a N terminal domain present in other MHV strains, has immunoevasive properties, and is a component of the virion. Genetic deletion of JHMV I (rJHMV^{IΔ57-137}) resulted in a highly attenuated virus both *in vitro* and in vivo that displayed a post RNA replication/transcription defect that ultimately resulted in fewer infectious virions packaged compared with wild-type virus. This phenotype was only seen for rJHMV^{IΔ57-137}, suggesting the structural changes predicted for A59 I altered its function, as genetic deletion of A59 I did not change viral replication or pathogenicity. Together, these data show that JHMV I both acts as a mild innate immune antagonist and aids in viral assembly and infectious virus production, and suggest that the internal N proteins from different betacoronaviruses have both common and virus strain-specific properties.

IMPORTANCE CoV accessory genes are largely studied in overexpression assays and have been identified as innate immune antagonists. However, functions identified after overexpression are often not confirmed in the infected animal host. Furthermore, some accessory proteins are components of the CoV virion, but their role in viral replication and release remains unclear. Here, we utilized reverse genetics to abrogate expression of a conserved CoV accessory gene, the internal N ("I") gene, of the neurotropic JHMV strain of MHV and found that loss of the I gene resulted in a post replication defect that reduced virion assembly and ultimately infectious virus production, while also increasing some inflammatory molecule expression. Thus, the JHMV I protein has roles in virion assembly that were previously underappreciated and in immunoevasion.

KEYWORDS coronavirus, innate immunity, mouse hepatitis virus, virion structure, encephalitis

Members of the *Orthocoronavirinae* subfamily of viruses share multiple conserved genomic features including structural genes and non-structural genes that are essential for viral assembly and replication, respectively. In addition, each coronavirus (CoV) encodes a unique set of accessory genes historically characterized as innate immune antagonists. Interestingly, there is one shared accessory gene in the genus *Betacoronavirus* that is expressed by several highly pathogenic human CoVs including

Editor Shan-Lu Liu, The Ohio State University, Columbus, Ohio, USA

Address correspondence to Stanley Perlman, stanley-perlman@uiowa.edu.

The authors declare no conflict of interest.

See the funding table on p. 21.

Received 7 June 2024 Accepted 4 July 2024 Published 19 August 2024

Copyright © 2024 American Society for Microbiology. All Rights Reserved.

September 2024 Volume 98 Issue 9

severe acute respiratory CoV (SARS-CoV), SARS-CoV-2, and Middle East respiratory syndrome CoV (MERS-CoV) as well as the prototypic Betacoronavirus, mouse hepatitis virus (MHV). Betacoronaviruses share an internal N gene, which is translated in the +1 open reading frame (ORF) of the nucleocapsid gene via leaky ribosomal scanning (1). The gene is designated I in MHV, ORF8b in MERS-CoV (called "8b" herein), and ORF9b in SARS-CoV-2 (called "9b" herein). Overexpression data indicate that 8b and 9b function as innate immune antagonists capable of altering interferon responses, inflammatory cytokine, and chemokine expression and disrupting the mitochondria; however, whether these functions contribute to viral pathogenicity in vivo has been largely unstudied (2-5). We recently showed that genetic deletion of MERS-CoV 8b results in increased pathogenicity in animals (6). 8b is a potent interferon antagonist in vitro and in vivo; loss of 8b leads to significantly increased levels of type 1 interferon (IFN-I) in the lungs of infected mice, resulting in a heightened inflammatory state coincident with enhanced lethality (6). In contrast, genetic deletion of SARS-CoV-2 9b attenuated viral replication in vitro and in vivo, with the lungs of 9b KO-infected mice showing mild increases of IFN-I expression (6). These data indicate that while the internal N gene is conserved across betacoronaviruses in genomic location, the function and effect on viral pathogenicity vary extensively.

While accessory genes are mostly studied for immune antagonism, there is evidence to suggest that they may play additional roles in maintaining virion integrity. Multiple SARS-CoV accessory proteins were shown to localize within the virion including ORF3a, 3b, 6, 7a, and 9b (7-12). In addition, an accessory gene knockout SARS-CoV (lacking 6, 7a, 7b, 8a, 8b, and 9b) had altered virion morphology in comparison to the wild type (WT); however, the specific accessory gene contributing to this phenotype remains unidentified (13). Genetic deletion of the I gene in the hepatotropic/neurotropic A59 strain of MHV (A59) did not result in altered virus replication, but A59 I was shown to be a minor structural protein present in the virion (1). Whether MHV I genes share similar innate immune antagonistic functions to those of 8b and 9b or whether the I gene contributes to virion integrity is not known. In addition, the I protein of the neurotropic JHM strain of MHV (JHMV) is truncated compared with that of A59, lacking a disordered N-terminus loop found in the I protein of multiple well-studied MHV strains. In order to address these questions, we genetically deleted the I gene of the neurotropic JHMV strain, assessed its function in vitro and in vivo, and compared its function to that of A59 I. Deletion of the JHMV I gene significantly attenuated virus replication in vitro and in vivo, with the most pronounced differences observed in interferon-competent settings. In addition, we determined that the JHMV I gene is a minor structural protein that supports infectious virion assembly and production.

RESULTS

Loss of I attenuates viral replication

Little is known about the function of the I gene in MHV. Previous genetic deletion of the A59 I gene resulted in no differences in replication both *in vitro* and *in vivo* (1). When we aligned the MHV I genes from commonly used laboratory strains MHV-1, -2, -3, -A59, and -JHMV, we found that the JHMV I gene encodes a premature stop codon and a second initiation codon that resulted in an N terminal-deleted protein (deleted by 71aa), making the JHMV I gene the shortest of these MHV strains (Fig. 1A; Fig. S1A). JHMV I is 77.8% genetically similar to A59 I and structural predictions indicated that this truncation disrupted a large, disordered loop at the N-terminus, while the long alpha helix was maintained in the C-terminus (Fig. 1B; Fig. S1B and C). Interestingly, the predicted structure of JHMV I was similar to that predicted for MERS-CoV 8b (6), despite minimal sequence similarity (30.93%) between these two proteins (Fig. S1D). To assess the function of JHMV I, we generated a recombinant JHMV I partial knockout (KO) virus (rJHMVI^{\text{\text{A57-137}}}), by introducing two nonsense mutations L56* and L73* into the I ORF to abrogate expression (Fig. 1A). We verified that genetic disruption of I did not disrupt nucleocapsid protein expression (Fig. S2A) and confirmed that the mutations were

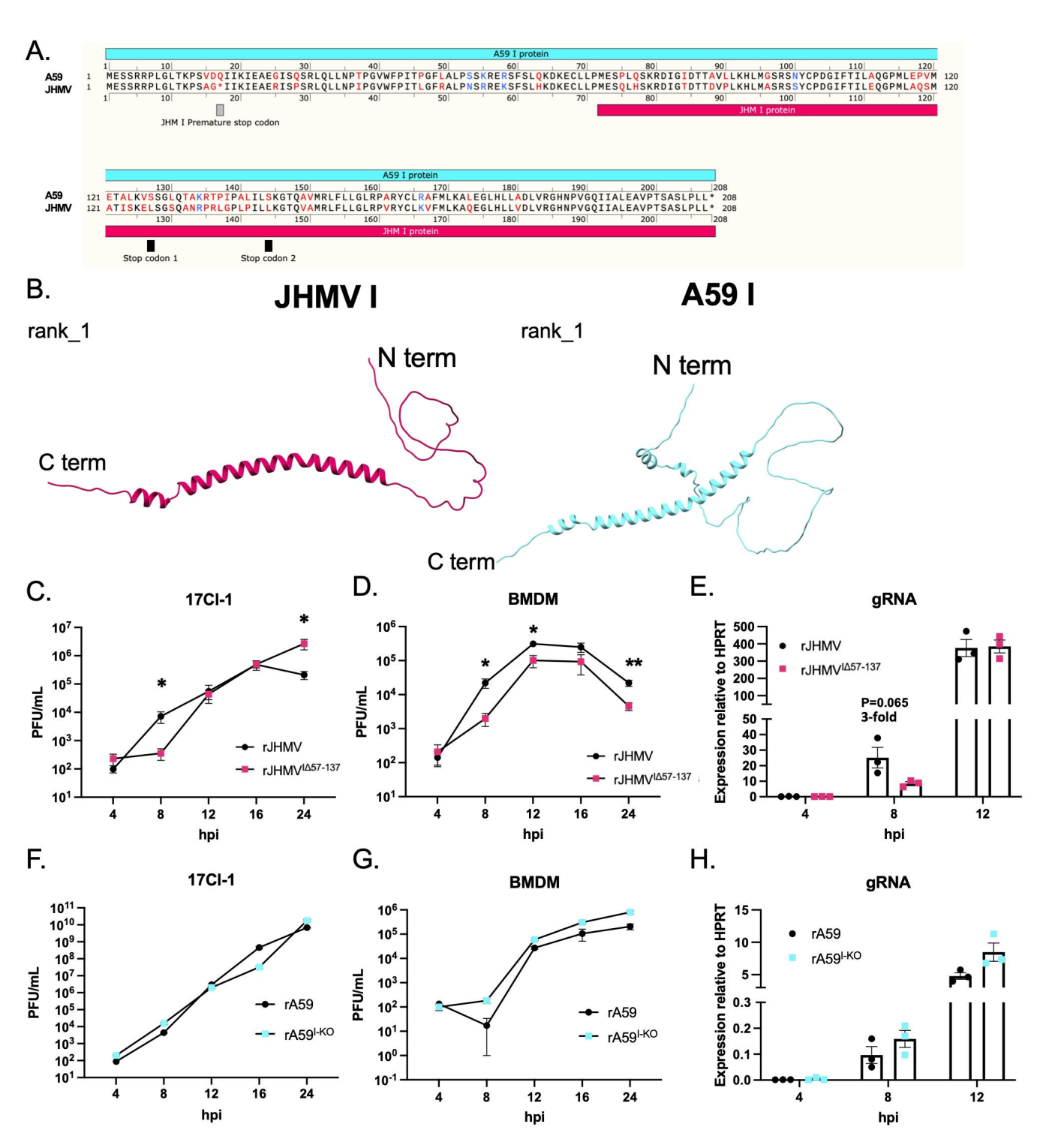


FIG 1 Loss of JHMV I protein results in attenuated replication. (A) Clustal omega sequence alignment of A59 (cyan) and JHMV I (magenta) proteins. Gray bar marks JHMV I termination codon that results in shortened protein. Black bars mark where L56* and L73* stop codons were introduced into rJHMV and and large blue residues indicate sequence dissimilarity with red representing no similarity and blue representing conserved side chains. (B) AlphaFold predicted structure rank #1 of JHMV I (magenta) and A59 I (cyan). (C) 17CI-1s or (D and E) BMDM were infected with rJHMV and rJHMV at 0.01 multiplicity of infection (MOI). (C and D) Cell lysates and supernatants were assayed at indicated time points for infectious virus by plaque assay. (E) quantitative reverse transcriptase-PCR (qRT-PCR) for gRNA. (F) 17CI-1s and (G and H) BMDMs were infected with rA59 and rA59 I-KO at 0.01 MOI. (F and G) Cell lysates and supernatants were plaque assayed at the indicated time points for infectious virus. (H) qRT-PCR for gRNA. The data in C-H are shown from one experiment representative of three independent experiments: n = 3 biological replicates. *P < 0.05 and **P < 0.01.

maintained through sequencing of the I gene. I protein expression could not be verified as antibodies against JHMV I are unavailable. We first evaluated rJHMVI^{Δ57-137} replication in 17Cl-1 cells, a mouse fibroblast cell line with minimal interferon expression. rJHMV^{IΔ57-137} was attenuated compared with WT rJHMV (rJHMV) at 8 hpi, but replication caught up and exceeded WT levels by 24 hpi. (Fig. 1C). In order to address if JHMV I is an interferon antagonist, we infected mouse bone marrow-derived macrophages (BMDMs), which are interferon competent and found that viral titers were significantly attenuated at almost all time points after infection with rJHMV (Fig. 1D). This phenotype was further confirmed by generating a second independent isolate of the rJHMV^{IΔ57-137} (rJHMV^{IΔ57-137 #2}) to confirm reduced replication was directly related to loss of the I gene and not a second site mutation (Fig. S2B). Notably, we observed that viral genomic RNA (gRNA) levels were not significantly decreased in the rJHMV^{IΔ57-137}infection (fold changes between 1.5 and 5; threefold change shown in Fig. 1E.) in contrast to differences observed in levels of infectious virus, suggesting viral attenuation occurred during assembly or release from cells (Fig. 1E). Previous evidence showed that rA59^{I-KO}, which expressed a full knock out of the I protein (1), was not defective in viral replication in vitro or in vivo relative to WT virus, but only a single time point was analyzed in this report (1). Since rJHMV^{IΔ57-137} attenuation was cell type dependent, we assessed infection with rA59^{I-KO} in 17CL-1 cells and BMDM. Deletion of the A59 I protein resulted in no significant attenuation of replication in either cell type, indicating that A59 I does not play a critical role in infectious virus production and does not appear to have substantial anti-IFN activity (Fig. 1F through H). These data indicate truncated JHMV I protein has altered function relative to the full-length I protein found in A59 and acts as a virulence factor that promotes viral replication, particularly in interferon-competent cells.

rJHMV I is a mild innate immune antagonist

In order to further determine the impact of rJHMV I on the interferon response, we collected RNA from BMDMs infected with rJHMV or rJHMV $^{\text{I}\Delta57-137}$ (MOI of 1) at 8 hpi and compared expression of IFN-I along with other inflammatory cytokines and chemokines by qRT-PCR. Despite a log reduction in viral titers of rJHMV $^{\text{I}\Delta57-137}$ to rJHMV at 8 hpi, all IFN-I, cytokines, and chemokines measured were equally or more highly expressed in rJHMV $^{\text{I}\Delta57-137}$ -infected cells with the exception of IFN- β (Fig. 2A). We saw statistically significant increases in ISG15, CCL2, and CXCL10 expression in rJHMV $^{\text{I}\Delta57-137}$ compared with rJHMV-infected cells (Fig. 2A). Infection of BMDMs with rA59 $^{\text{I-KO}}$ at an MOI of 1 also showed increased expression of IFN-a, ISG15, and CXCL10 compared with rA59 (Fig. 2B). These data indicate that the MHV I proteins are mild innate immune antagonists similar to MERS-CoV ORF8b and SARS-CoV-2 ORF9b, only affecting a subset of inflammatory molecules. However, the impact this plays in pathogenicity remains to be addressed.

rJHMV^{I∆57-137} is significantly attenuated in vivo

Given these results, we next determined the effect of the absence of the JHMV I protein after infection of mice. JHMV causes a lethal encephalitis in most strains of mice (14). Five- to seven-week-old C57BL/6 mice were infected intranasally with a lethal dose of rJHMV. Animal weights, survival, and clinical disease (signs of encephalitis and demyelination) were evaluated daily. rJHMV^{IΔ57-137}-infected mice exhibited reduced weight loss and increased survival relative to rJHMV-infected mice (Fig. 3A). Roughly 60% of rJHMV^{IΔ57-137}-infected animals survived compared with 100% mortality of rJHMV-infected mice (Fig. 3A). Interestingly, while rJHMV-infected mice only displayed signs of acute encephalitis (ruffled fur, lethargy, and limited mobility) prior to reaching endpoint euthanasia, a subset of rJHMV^{IΔ57-137} mice had symptoms of both acute encephalitis and demyelination (hind limb paresis/paralysis). This pattern of disease closely resembled those observed after infection with the neuroattenuated J2.2.V-1 strain of rJHMV (15). The rJHMV-J2.2.V-1 strain encodes a spike mutation that alters infection from neurons to glial cells, resulting in preferential oligodendrocyte infection and dewyelination (15, 16). Ninety percent of J2.2.V-1-infected animals survive infection and develop hind limb

September 2024 Volume 98 | Issue 9 10.1128/jvi.00680-24 **4**

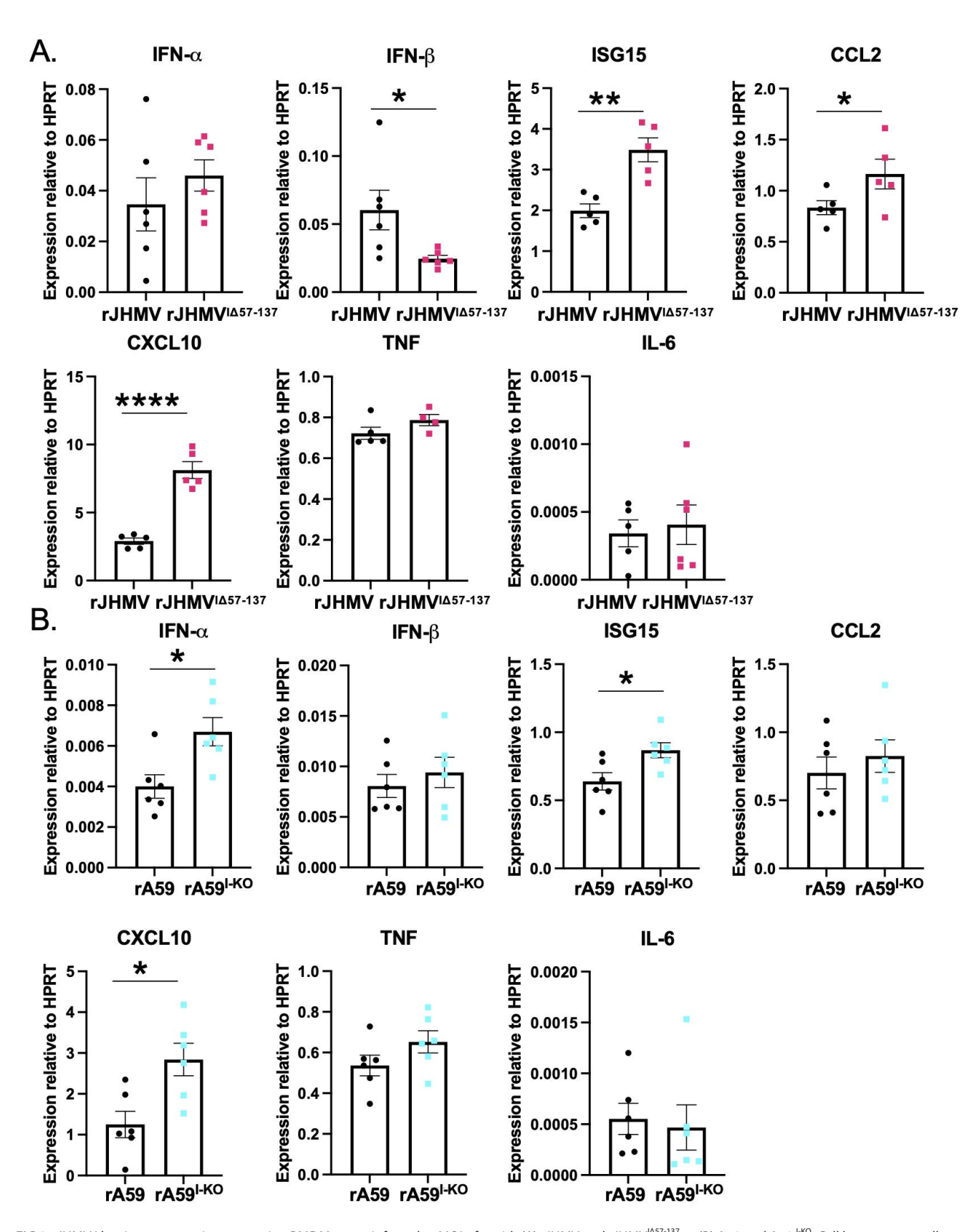


FIG 2 JHMV I has immunoevasive properties. BMDMs were infected at MOI of 1 with (A) rJHMV and rJHMV I has immunoevasive properties. BMDMs were collected at 8 hpi for measurement by qRT-PCR of mRNA levels of immune mediators IFN-a, IFN-b, ISG15, CCL2, CXCL10, TNF, and IL-6. The data from one experiment representative of two independent experiments are shown: n = 6 biological replicates. *P < 0.05 and **P < 0.01.

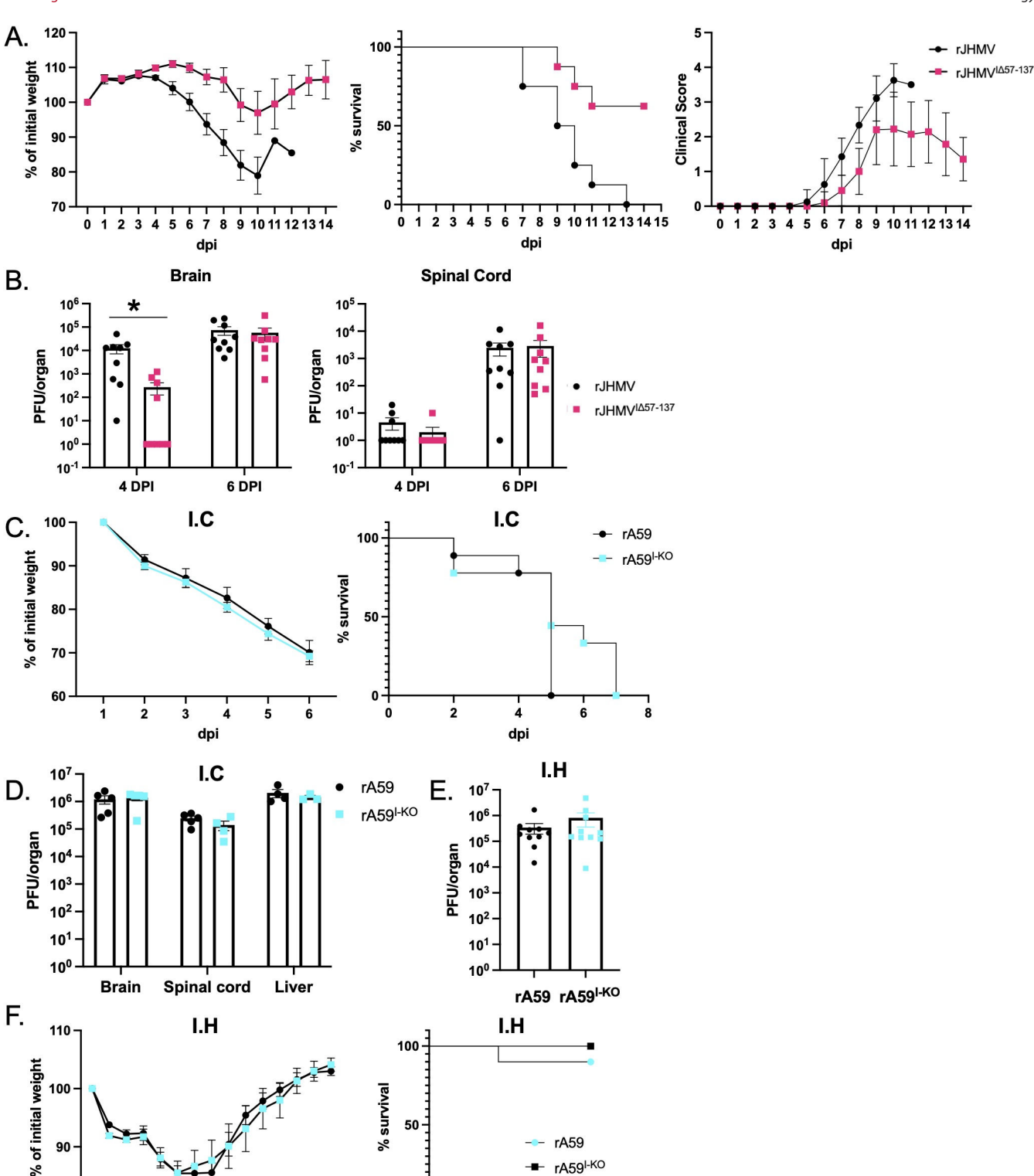


FIG 3 Pathogenicity is attenuated in rJHMV^{\(\Delta z 7-137\)}-infected mice. (A and B) Five- to seven-week-old C57L/B6 mice were infected intranasally with 60,000 $PFU/12~\mu L~rJHMV~or~rJHMV^{l\Delta57-137}.~Animal~weights,~survivability,~and~clinical~scores~were~evaluated.~(B)~Whole~brain~and~spinal~cord~were~harvested~at~indicated~and~clinical~scores~were~evaluated.~(B)~Whole~brain~and~spinal~cord~were~harvested~at~indicated~at$ time points and homogenized, and infectious virus titers were measured by plaque assay. (C and D) Five- to seven-week-old C57L/B6 mice were infected with 30,000 PFU/30 µL of rA59 and rA59 intracranially. Animal weights and survival were evaluated. (D) Whole brain, spinal cord, and liver were harvested at 4 (Continued on next page)

8 10

dpi

12 14

80

ò 2 12 14

10

dpi

FIG 3 (Continued)

dpi and homogenized, and infectious virus titers were measured by plaque assay. (E) Five- to seven-week-old C57L/B6 mice were infected intrahepatically with 10,000 PFU/300 μ L of rA59 and rA59 ^{I-KO}, and whole liver was harvested a 2 dpi and homogenized, and infectious virus was measured by plaque assay. (F) Five-to seven-week-old C57L/B6 mice were infected intrahepatically with 10,000 PFU/300 μ L of rA59 and rA59 ^{I-KO} and weighed daily. (A and C) One representative experiment from three independent experiments is shown: n = 8-10 biological replicates. (B) Two independent experiments were combined n = 9. (D) One representative experiment of three independent experiments: n = 4-5. (E and F) Two experiments combined: n = 10.*P < 0.05.

paresis/paralysis before recovering. Clinical scoring showed that rJHMV^{IΔ57-137}-infected mice had delayed onset of clinical signs and did not fully recover by 14 days post-infection (dpi) (Fig. 3A). To further analyze the nature of this attenuation and its impact on viral kinetics, we evaluated viral titers in the brain and spinal cord at multiple time points post-infection. At 4 dpi, rJHMV^{IΔ57-137}-infected mice had significantly less virus in the brain compared with rJHMV-infected counterparts (Fig. 3B). However, by 6 dpi, rJHMV^{IΔ57-137} reached equivalent titers to rJHMV. In the spinal cord, replication was identical between rJHMV- and rJHMV^{IΔ57-137}-infected mice, potentially reflecting the fact that while replication is delayed in the brain, viral titers reach similar levels between 4 and 6 dpi, coinciding with the time at which virus enters the spinal cord (Fig. 3B).

A59 is predominantly a hepatotropic virus. First, however, we inoculated animals intracranially with a lethal dose of rA59 and rA59^{I-KO} to assess viral replication in the brain and spinal cord, to parallel experiments with rJHMV. We found no differences in weight loss or mortality (Fig. 3C). In addition, viral titers of the brain, spinal cord, and liver were equivalent at 4 dpi after intracranial infection with rA59 and rA59^{I-KO} (Fig. 3D). In order to confirm this phenotype was not inoculation route or brain infection dependent, we infected animals intrahepatically with rA59 and rA59^{I-KO} and again found no difference in viral titers in the liver (Fig. 3E) or animal survival (Fig. 3F). Overall, loss of A59 I did not alter A59 replication or pathogenicity significantly *in vitro* or *in vivo*.

The significant delay in viral kinetics after infection with rJHMV^{IΔ57-137} (Fig. 3B) prompted us to evaluate immune cell infiltration into the brains of rJHMV^{IΔ57-137}-infected mice. Flow cytometry was used to assess the degree and composition of immune cell infiltration at 4 and 6 dpi, as innate immune cells begin infiltrating the brains of rJHMV-infected mice as early as 2 dpi (16). rJHMV-infected mice showed a greater influx of immune cells at 4 dpi compared with rJHMV^{IΔ57-137} which only reached comparable cell frequency and numbers by 6 dpi, while the resident brain microglia populations remained comparable (Fig. 4B through D; gating shown in Fig. 4A). CD45+ CD11b+ cells were reduced in both frequency and number by fourfold in rJHMV^{\(\Delta 57-137\)}-infected animals at 4 dpi (Fig. 4D). This included a significant reduction of both the frequency and number of infiltrating monocytes/macrophages and neutrophils (four- and threefold, respectively) in rJHMV^{IΔ57-137}-infected mice compared with rJHMV (Fig. 4E and F). CD45+ CD11b- cells were also significantly reduced (fourfold) in rJHMV^{IΔ57-137}-infected mice; however, T cells were not similarly reduced despite delayed viral kinetics and innate immune cell infiltration (Fig. 4G). These data indicated that the adaptive immune response was not delayed and may promote survival in $rJHMV^{l\Delta57-137}$ -infected mice. Collectively, these in vivo data clearly demonstrated a significant attenuation of disease and infection kinetics in rJHMV^{IΔ57-137} relative to rJHMV-infected mice. Flow cytometric analysis of immune cell infiltration into the brains of rA59-infected mice at 4 dpi revealed increased number of both innate and adaptive immune cells in rA59^{I-KO}-infected mice; however, the basis of this alteration in cellular infiltration is unclear (Fig. 5). These disparate outcomes further demonstrate that JHMV I compared with A59 I protein has a differential impact on pathogenicity and that the absence of JHMV I severely attenuates viral replication and delays the subsequent immune response. The consequence of this delay is that there is sufficient time for mounting an effective adaptive immune response, thereby, improving the overall outcome of rJHMV^{IΔ57-137}-infected animals.

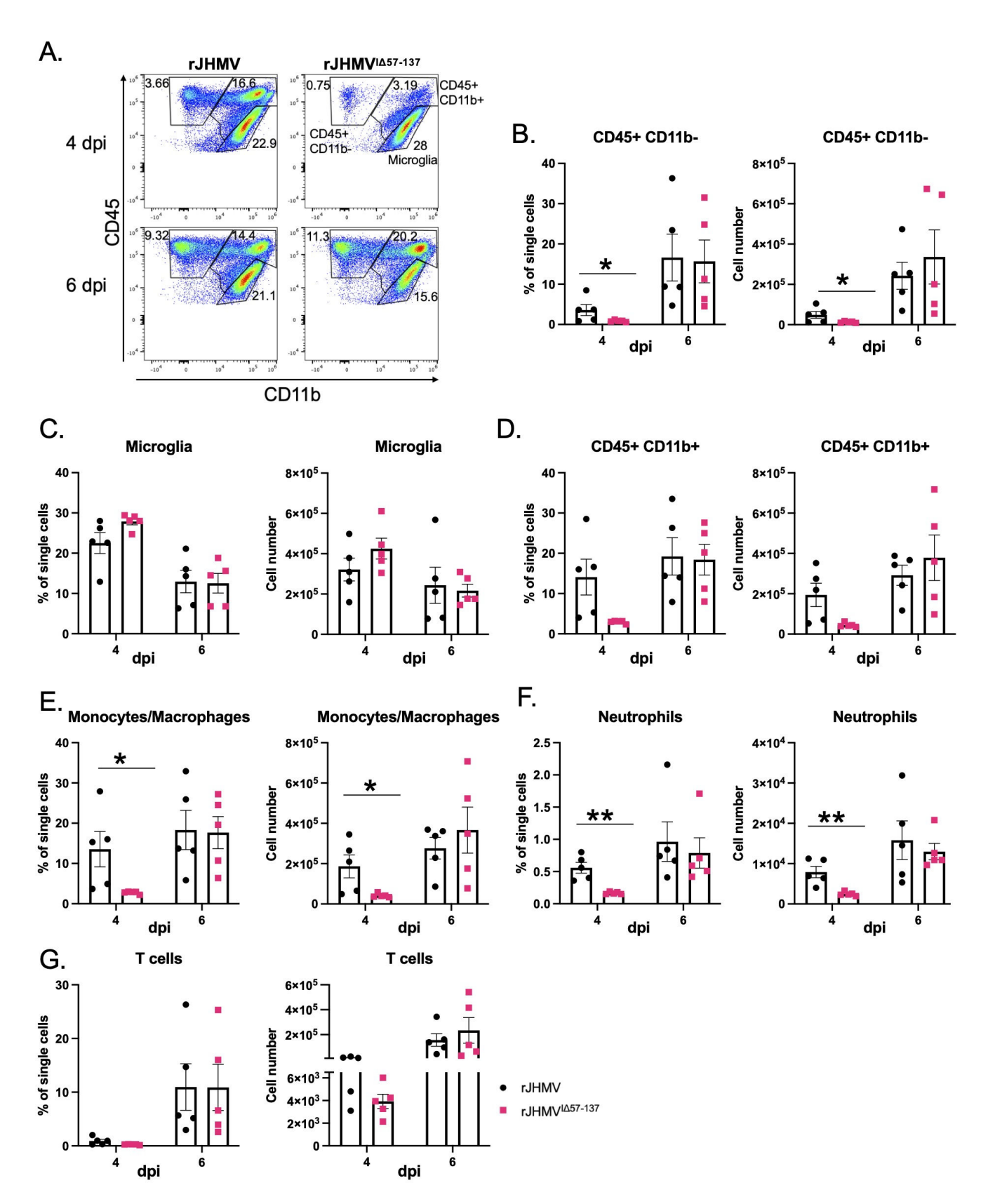


FIG 4 Immune cell infiltration is delayed in rJHMVI⁰⁵⁷⁻¹³⁷-infected mice. (A) Five- to seven-week-old C57L/B6 mice were infected intranasally with 60,000 PFU/12 µL of rJHMV or rJHMV ^{\(\Delta 57-137\)}, and brains were collected at indicated time points and processed for flow cytometry. Representative flow plots to show gating of CD45- (y-axis) vs CD11b- (x-axis) positive cells at 4 and 6 dpi. (B) Frequency and number of CD45+ CD11b- cells. (C) CD45^{int}CD11b+ microglia. (D) CD45+ CD11b+ cells. (E) CD45+ CD11b+ Ly6G- monocytes and macrophages. (F) CD45+ CD11b+ Ly6G+ neutrophils. (G) CD45+ CD11b- CD3+ T cells. One representative experiment from three independent experiments is shown: n = 4-5. *P < 0.05 and **P < 0.01. September 2024 Volume 98 Issue 9

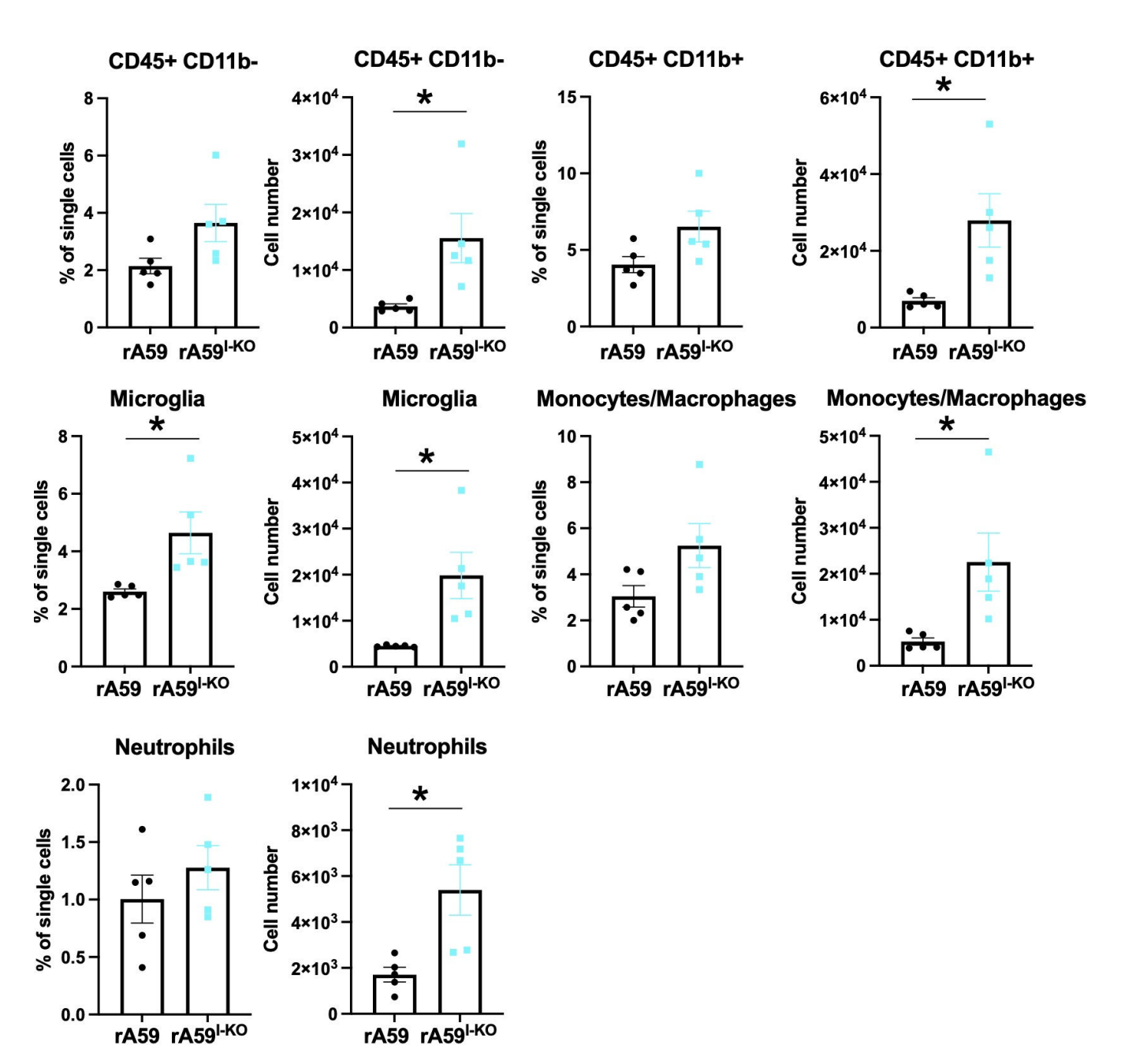


FIG 5 Immune cell infiltration is modestly increased in A59^{I-KO}-infected mice. Five- to seven-week-old C57L/B6 mice were infected with 30,000 PFU/30 μ L of rA59 and rA59^{I-KO} intracranially. Brains were collected at indicated time points and processed for flow cytometry. Frequency and count of CD45+ CD11b- cells, CD45 intermediate CD11b+ microglia, CD45+ CD11b+ cells, CD45+ CD11b+ Ly6G- monocytes and macrophages, and CD45+ CD11b+ Ly6G+ neutrophils. These data are obtained from two independent experiments: n = 4-5. *P < 0.05.

rJHMV^{I∆57-137} does not solely function as an interferon antagonist

rJHMV^{IΔ57-137}growth was significantly attenuated in interferon-competent cell lines *in vitro*, and JHMV I displayed IFN-I antagonism at the RNA expression level (Fig. 1D and 2A). We next evaluated if the attenuated replication of rJHMV^{IΔ57-137} was solely a consequence of the loss of interferon antagonism. For this purpose, we infected IFN-alpha/beta receptor knockout (IFNAR^{-/-}) BMDMs with rJHMV and rJHMV^{IΔ57-137} and evaluated growth kinetics in the absence of IFN signaling. We hypothesized that if the predominant function of I was interferon antagonism, replication of rJHMV and rJHMV^{IΔ57-137} should be similar in cells or mice lacking IFN-I signaling; however, this was not the case. Even in

the absence of IFN-I signaling, rJHMV^{IΔ57-137} was significantly attenuated compared with rJHMV (Fig. 6A), although the differences were not as profound as observed in infected WT BMDM. These data support the conclusion that IFN-I antagonism is not the sole factor in rJHMV^{IΔ57-137} attenuation (Fig. 6A). Interestingly, infection of IFNAR^{-/-} mice with rJHMV or rJHMV^{IΔ57-137} resulted in identical weight loss and mortality (Fig. 6B). However, when we evaluated viral replication at 4 dpi, we found that viral loads in the spinal cords of rJHMV^{IΔ57-137}-infected mice were significantly reduced (Fig. 6C). Similar results were obtained when infected brains were analyzed, although these differences did not reach significance. We assessed whether the rA59^{I-KO} infection would be affected in IFNAR^{-/-} BMDM; however, we saw no differences in viral replication between rA59^{I-KO} and rA59 (Fig. 6D). These data indicate attenuation of the rJHMV^{IΔ57-137} is multi-faceted and that I protein is not solely immunoevasive.

JHMV I is essential for virion integrity

While the experiments above demonstrate JHMV and A59 I proteins have partially non-overlapping functions in replication and pathogenicity, it is not yet clear what contributes to these differences. We hypothesized that the truncation in JHMV I that results in a lack of the disordered loop in the N terminus of A59 and other MHV strain I proteins may have altered I protein localization in infected cells. Since there is no commercially available antibody for JHMV I, we generated viruses wherein the JHMV or A59 I genes were tagged with V5 and inserted into ORF4 of the rJHMV backbone (rJHMV^{JHM-I} and rJHMV^{A59-I} herein) (Fig. 7A). We previously showed that deletion of ORF4 does not alter viral replication or pathogenicity and is a site for stable gene insertion (17). V5 tag expression was verified by western blot analysis for both viruses (Fig. 7B). A time course of rJHMV^{JHM-I} revealed I-V5 expression at 8 and 12 hours, with expression waning

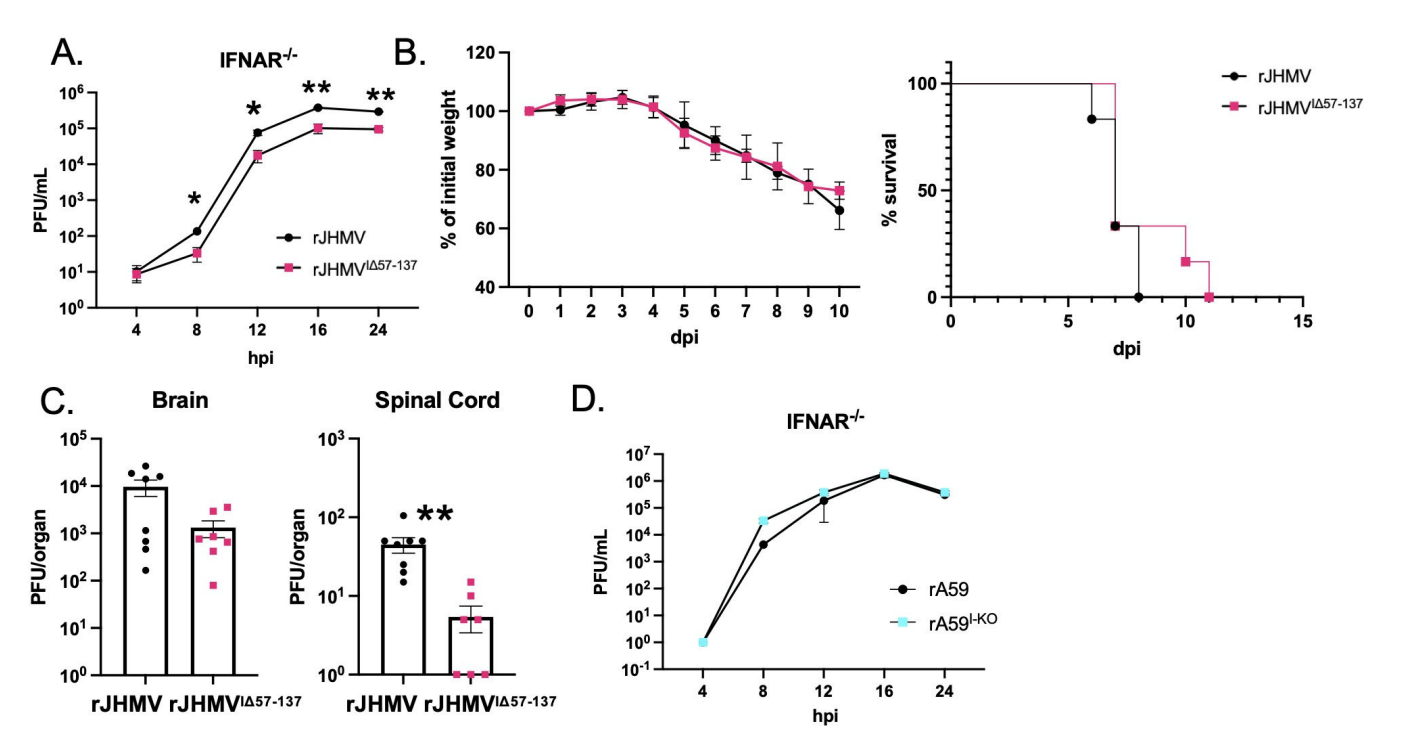


FIG 6 rJHMV $^{\Delta 57-137}$ attenuation is partially reversed in IFNAR $^{-/-}$ mice. (A) IFNAR $^{-/-}$ BMDM were infected with rJHMV and rJHMV $^{\Delta 57-137}$ at 0.01 MOI. Cell lysates and supernatants were prepared and analyzed at the indicated time points by plaque assay for infectious virus. (B and C) Five- to seven-week-old IFNAR $^{-/-}$ mice were infected intranasally with 20,000 PFU/12 μL of rJHMV and rJHMV $^{\Delta 57-137}$, and weight and survival were monitored. (C) Whole brains and spinal cords were harvested at 4 dpi and homogenized, and infectious virus was measured by plaque assay. (D) IFNAR $^{-/-}$ BMDM were infected with A59 and A59 $^{1-KO}$ at 0.01 MOI. Cell lysates and supernatants were prepared and analyzed at the indicated time points for infectious virus. The data in A and D were obtained from one experiment representative of three independent experiments: n = 3 biological replicates. The data in B are two combined from independent experiments n = 7 and those in C are combined from two independent experiments n = 7-8. *P < 0.05 and **P <

10.1128/jvi.00680-24 **10**

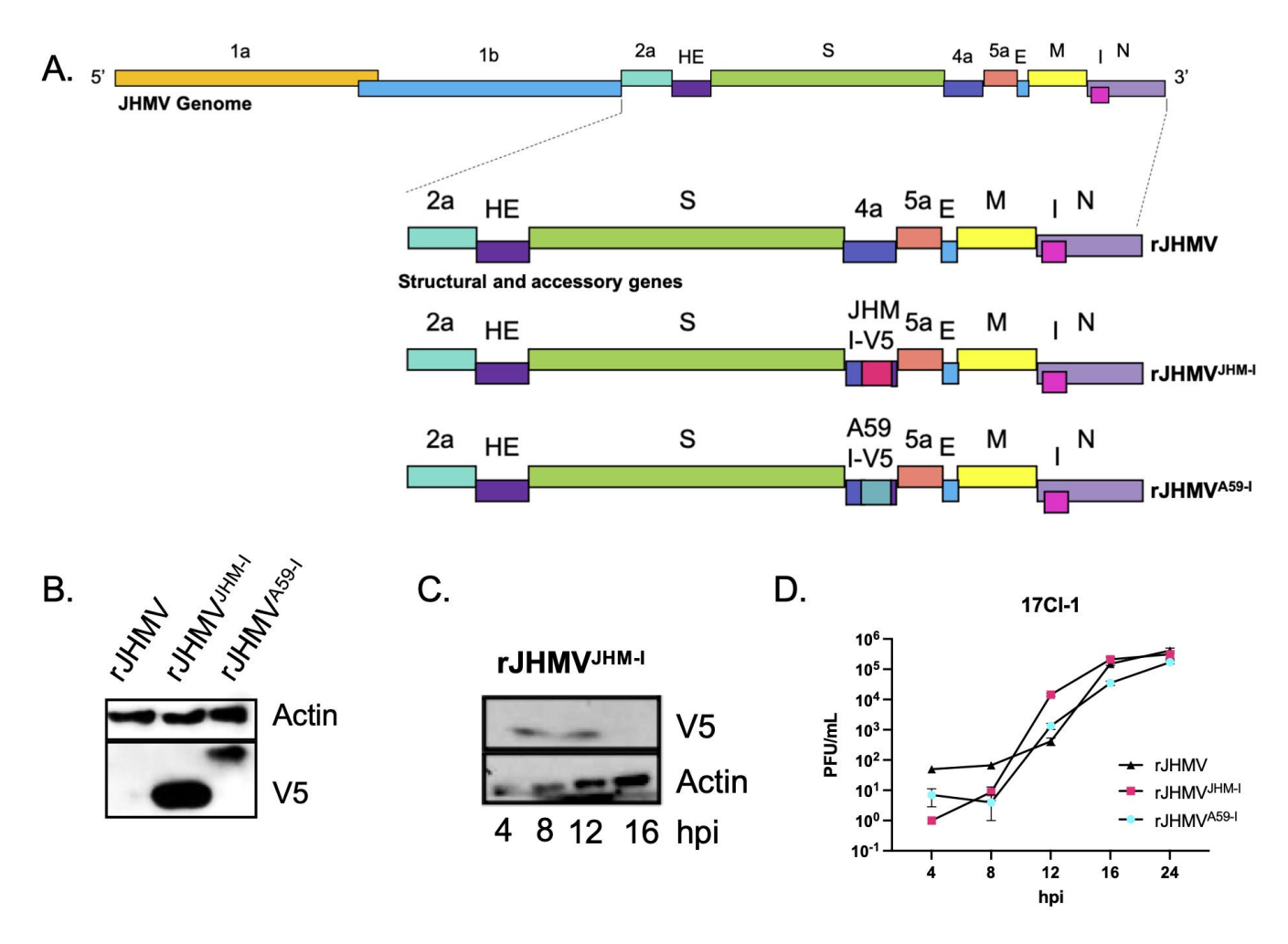


FIG 7 Generation and analysis of V5-tagged JHMV I and A59 I viruses. (A) Schematic of JHMV genome with 3' end amplified to show insertion of the V5-tagged MHV I within ORF4. (B) 17CI-1s were infected with 0.01 MOI of rJHMV, rJHMV^{JHM-I}, or rJHMV^{A59-I}. Cell lysates were collected at 12 hpi for western blot probing V5 tag and actin. (C) 17CI-1s were infected with 0.01 MOI of rJHMV^{JHM-I}. V5 and actin were probed at 4, 8, 12, and 16 hpi. (D) 17CI-1s were infected with 0.01 MOI of rJHMV, rJHMV^{A59-I}. Cell lysates and supernatants were plaque assayed at the indicated time points for infectious virus. The data in B–D were obtained from one experiment representative of three independent experiments: *n* = 3 biological replicates.

by 16 hpi (Fig. 7C), similar to the expression of MERS-CoV ORF8b (6). Additionally, viral replication kinetics were similar between the rJHMV and tagged viruses (Fig. 7D).

We utilized confocal microscopy to compare I protein localization in cellular organelles associated with CoV virion assembly. Both the JHMV and A59 I protein showed strong colocalization with a cis Golgi matrix protein (GM-130) with Pearson coefficient values above 0.7 (Fig. 8A). I protein fluorescence expanded beyond the Golgi to areas considered ER Golgi intermediate compartment (ERGIC), which is considered the major CoV budding compartment (18, 19). The punctate patterns in the cytoplasm moderately overlapped with ER protein regions (Pearson's coefficient of 0.3 for rJHMV^{JHM-1} and 0.5 for rJHMV^{A59-I}) (Fig. 8B). Similar colocalization to the Golgi and ERGIC has been reported for CoV proteins that localize to the virion including structural proteins such as M and other accessory proteins (18, 20, 21). These data suggest that JHMV I has a previously unappreciated role in virion assembly. It was previously shown that 9b, and to a lesser extent, 8b, interacted with the mitochondrial protein, TOM70, and altered mitochondria function (5, 6, 22). We performed colocalization of I protein with TOM70 and did not see significant colocalization (Pearson's coefficient of 0.2 for rJHMV^{JHM-I} and 0.4 for rJHMV^{A59-I}) (Fig. 8C). Consistent with this observation, we were unable to detect a mitochondrial transit peptide sequence in either JHMV or A59 I. These data indicate JHMV I and A59

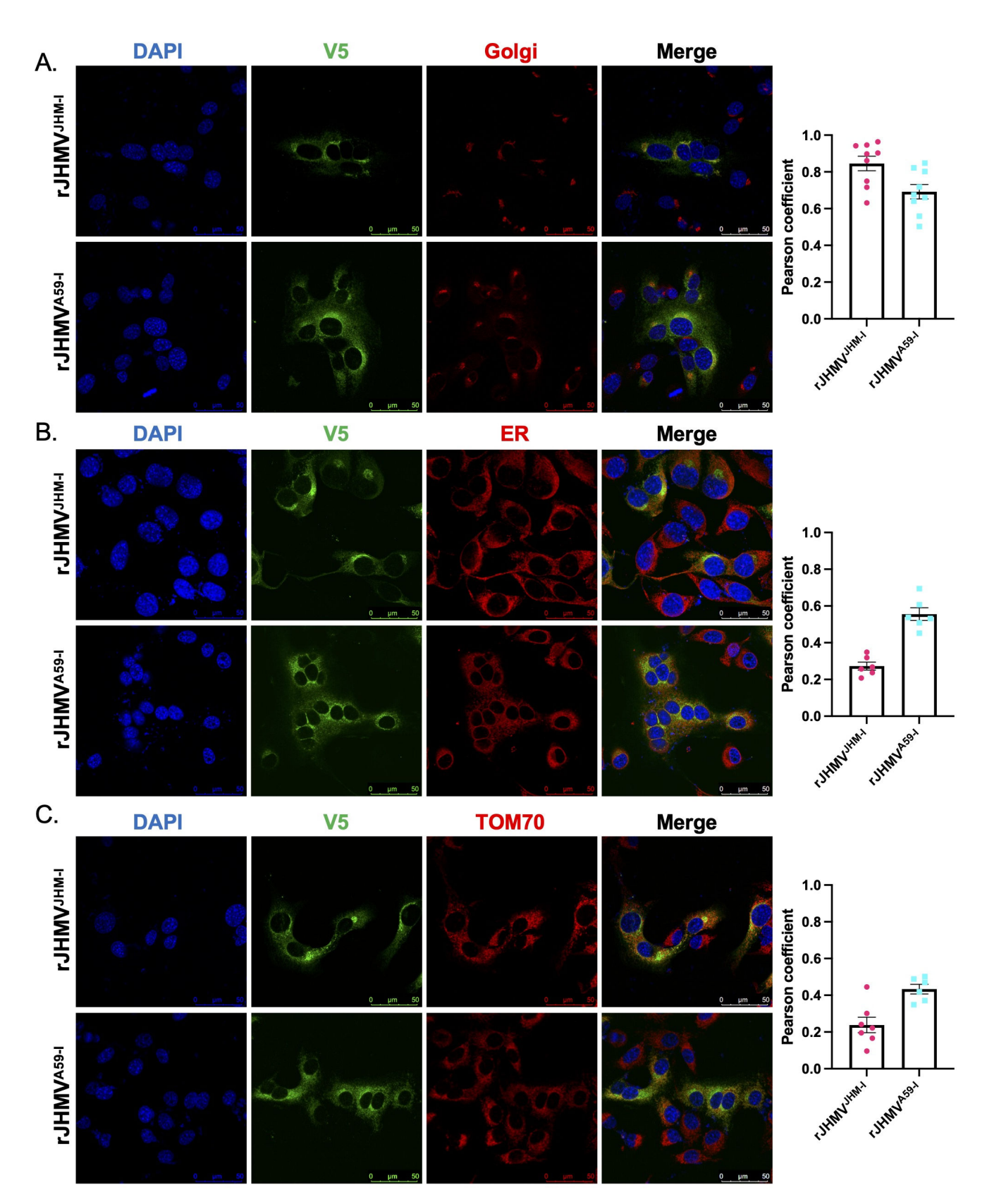


FIG 8 MHV I colocalizes to Golgi. 17CI-1s were infected with rJHMV^{JHM-I} (upper panels) or rJHMV^{A59-I} (lower panels) at 0.1 MOI and fixed at 8 hpi as described in Materials and Methods. Slides were stained for DAPI, V5 tag expression, and (A) Golgi, (B) ER, and (C) TOM70 and visualized by confocal microscopy. Each image is representative of 7–9 images, and Pearson coefficients were measured for 6–8 images with an average total of three infected cells per image.

I innate immune antagonism may be independent of the mitochondrial/ IFN-I signaling pathway.

To examine whether JHMV I assembled into the virion as a minor structural protein similar to what was observed in rA59-infected cells (1), 17CI-1 cells were infected at an MOI of 0.01 and harvested at 16 hpi. Virions were concentrated by centrifugation. Fractions were obtained and examined by western blot for spike and I protein expression. In addition, we measured viral titers to determine the fractions with the highest concentration of infectious virus. rJHMV^{JHM-I} I protein, assessed using anti-V5 antibody, was found most prominently in fractions 6, 7, and 8 which corresponded with peak viral titers and spike protein expression, suggesting that JHMV I is a component of the virion (Fig. 9A). Due to JHMV being 90% cell associated (23), we were unable to perform purification of supernatant virus because yields were low.

Given the presence of I protein in the virion and the relative equivalence of viral gRNA levels in rJHMV and rJHMV^{IΔ57-137}-infected cells, despite decreased infectious virus production, we questioned whether JHMV I protein was required for optimal infectivity. To interrogate this question, we infected BMDMs with rJHMV and rJHMV^{IΔ57-137} viruses and then performed plaque assays for infectious virus and qRT-PCR for gRNA levels at 12 hpi of both cell pellet and supernatant. We found the RNA levels within the cell pellet were similar (average CT value of 23.4 for rJHMV and 24.2 for rJHMV^{IΔ57-137}) but infectious virus was significantly reduced in rJHMV^{IΔ57-137}. Therefore, the ratio of RNA to PFU was significantly higher in rJHMV^{IΔ57-137}-infected cells in comparison to rJHMV (Fig. 9B). Interestingly, this affect was cell pellet specific, as viral RNA and infectious virus were equivalent in the supernatant. This suggested that the replication defect seen for rJHMV^{IΔ57-137} occurs between transcription and release of infectious particles.

Given these data and previous studies of SARS-CoV-infected cells demonstrating that deletion of accessory genes altered virion morphology, we next used electron microscopy (EM) to assess the morphology of rJHMV and rA59 and their respective I KO viruses. BMDM were infected at a 0.01 MOI and evaluated at 12 hpi. We did not see altered morphology when rJHMV and rJHMV^{lΔ57-137} particles were compared; however, we found significantly fewer particles in rJHMV^{IΔ57-137}-infected cells compared with rJHMV-infected cells (Fig. 9D, virions marked with magenta arrows). In addition, some of the Golgi organelles in rJHMV^{IΔ57-137}-infected cells were empty and distended (Fig. 9D, marked with a blue star) in comparison to those seen in rJHMV-infected cells which contained viruses (marked with white asterisk). Empty and dilated Golgi cisterna generally indicate a protein packaging defect (24). Furthermore, we did not find particles close to the plasma membrane suggesting that rJHMV^{IΔ57-137} attenuation was at the particle assembly step (24). No direct interaction was observed between rJHMV I and the nucleocapsid protein when assessed via co-immunoprecipitation (Co-IP) (Fig. 9C). Thus, it remains to be established whether rJHMV I interacts with a viral or host protein or viral RNA to facilitate virion assembly and egress. Electron microscopic examination of rA59- and rA59^{I-KO}-infected cells did not show morphological differences between virions (Fig. 9E). Virions from cells infected with either could be seen throughout the cell cytoplasm in large vesicles and in Golgi and ER membranes, indicating viral assembly proceeded as expected for these viruses, with the rA59^{I-KO} displaying significantly increased virions compared with WT when quantified (Fig. 9E, vesicles with virions marked with cyan asterisk). Overall, these data further support the conclusion that A59 I is a virion structural component but has a lesser or no role in viral assembly. In contrast, JHM I specifically is essential for optimal virion assembly. In rJHMV^{IΔ57-137}-infected cells, gRNA levels are equivalent to those in WT-infected cells, yet we see reduced particles via EM and reduced infectious virus production over time resulting in an increased RNA/PFU ratio. Thus, once virus is released from infected cells, specific infectivity was not impaired by the truncation of the I protein, indicating the virus is highly attenuated due to a reduction in particle assembly following genome transcription.

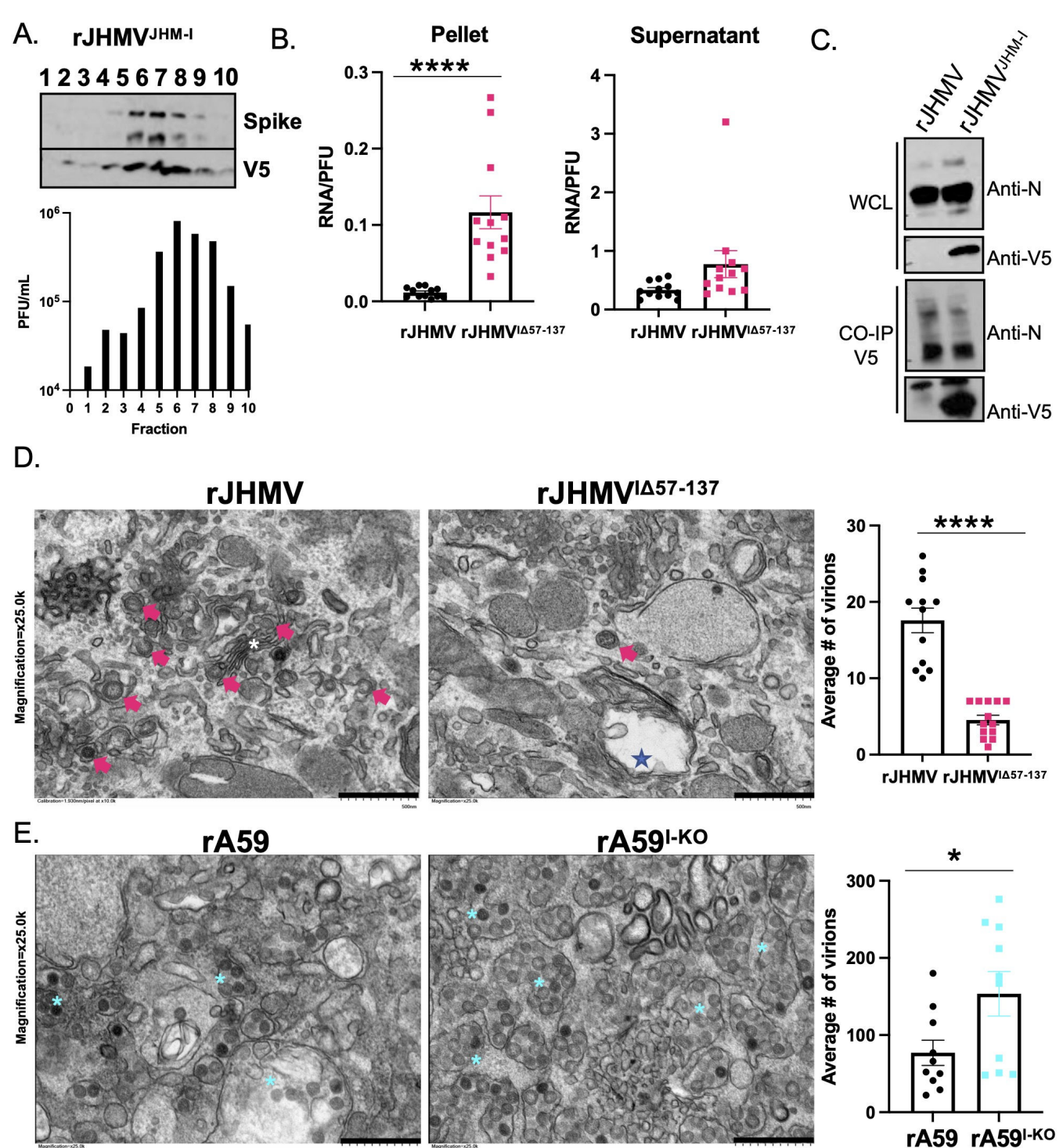


FIG 9 Absence of JHMV I reduces virus assembly and RNA/PFU ratio. 17CI-1s were infected with (A) rJHMV^{HMAI} at 0.01 MOI, and cells and supernatant were harvested at 16 hpi. Virions were concentrated via centrifugation and fractionated. Fractions were examined by western blot for spike and V5 protein expression, as well as viral titer by plaque assay. (B) BMDMs were infected with rJHMV and rJHMV^{IΔ57-137} at 0.01 MOI, and cells and supernatant were harvested at 12 hpi. Infectious virus and gRNA were measured by plaque assay and qRT-PCR, respectively. Ratio of RNA to plaque-forming unit (infectious virus) was measured. (C) Analysis of N and I binding. Infected cell lysates were collected at 12 hpi prepared and treated with anti-V5 antibody beads. Bound samples were eluted and analyzed for nucleocapsid and V5 expression. (D) Electron microscopy of BMDMs infected with (D) rJHMV and rJHMV^{IΔ57-137} or (E) A59 and A59^{I-KO} at 0.01 MOI and harvested at 12 hpi. Larger panels at 25k resolution with a scale bar of 500 nm and smaller panels at 50k resolution with a scale bar of 200 nm. Examples of rJHMV virions are marked with magenta arrows. Blebbed Golgi cisternae seen only in rJHMV^{IΔ57-137} marked with blue star. Golgi stacks containing virions marked with (Continued on next page)

FIG 9 (Continued)

white asterisk. Collections of vesicles containing virions only found in rA59-infected samples marked with cyan asterisk. Number of virions per field quantified blindly. The data in A were obtained from one experiment representative of three independent experiments: n = 1 biological replicates. The data in B are representative of two independent experiments, n = 12, those in C are representative of one independent experiment, and those in D and E are representative of two biological replicates, and n = 10–12 images quantified.

DISCUSSION

In this study, we showed that loss of JHMV I protein resulted in significant attenuation of replication and pathogenicity. rJHMV^{IΔ57-137} attenuation is twofold: (i) loss of innate immune antagonism and (ii) disrupted virus assembly, which results in reduced particle production. Prior to this study, evidence regarding the role of CoV accessory proteins in virion formation was limited. Some studies identified SARS-CoV accessory proteins as minor structural proteins within the virion. A single study examined the morphology of SARS-CoV lacking accessory genes 6, 7a, 7b, 8a, 8b, and 9b by EM and noted impaired virion morphology compared with wild-type virus (12). Here, we delved further into understanding the functional role of the MHV I protein in virion formation. We utilized tagged viruses to show that MHV I is associated with the Golgi apparatus, similar to that of other structural and accessory proteins associated with virion assembly (12, 18, 21). Assembly occurs at the ERGIC, which includes the late Golgi apparatus, the site of I protein accumulation in rJHMV-infected cells (Fig. 8A) (21). Furthermore, we determined that loss of the rJHMV I protein resulted in an increased RNA/PFU ratio relative to rJHMV, also consistent with a role of the I protein in virion assembly (Fig. 9B). To further probe the contribution of the I protein to virion assembly, we compared WT and I KO viruses via electron microscopy. EM of these viruses did not display alterations to virion morphology, as both WT and I KO viruses displayed spherical virions with an electron dense interior, consistent with the presence of viral nucleocapsid (Fig. 9C) (25). However, the Golgi cisterna were distended and dilated in rJHMV^{IΔ57-137}-infected cells and largely devoid of virions in comparison to rJHMV-infected cells. The significant reduction in viral particles while viral RNA remained equivalent further reinforced the conclusion that the absence of JHMV-I resulted in a packaging level defect. Previously, Li et al. showed that deletion of the alpha helix located in the C-terminus of MERS-CoV 8b resulted in decreased localization to the Golgi complex (26), suggesting that the conserved alpha helix in JHMV I and A59 I proteins is also required for Golgi association. However, localization to sites of virion assembly does not indicate that the protein has specific roles, as both JHMV and A59 I localize to these regions while infection with rA59^{I-KO} results in no loss of infectivity. These results suggest that virus strain-specific interactions with host and/or viral proteins aid in JHMV I function. These data provide clearer evidence of the importance of the I protein in CoV virion formation and raise questions about whether other CoV accessory proteins have similar functions.

The N terminus absent from JHMV I is the defining difference between JHMV I and the other MHV I proteins; however, the significance of this difference is not known. The N-terminus of 8b is required for optimal immune evasion, while its C-terminus engages in cellular localization (6, 26). We propose that the loss of the disordered N-terminus in JHMV I allows I protein to interact with host and/or viral proteins differently from A59 I. Consistent with this, less IFN-I antagonism was observed when A59- and JHMV-infected cells were compared (Fig. 2). In addition, A59 I structure rank_5, generated by AlphaFold (Fig. S1C), shows a break in the alpha helix that bends the alpha helix back onto the A59 I protein. This bend is facilitated by a proline located at that site. An alternative hypothesis is that the break in the alpha helix leads to the C-terminus of A59 I interacting with its N-terminus and inhibiting itself and possibly affecting binding to host/viral proteins. Interestingly, MERS 8b also encodes a stop codon that truncates the N-terminus of 8b in comparison to closely related viral strains HKU4 and HKU5 (2). It is possible that CoVs evolve their I proteins to better support viral replication perhaps in a host-dependent manner (2, 26).

Until recently, evidence that the betacoronavirus internal N gene acted as an innate immune antagonist was largely based on overexpression data, with only one study demonstrating that genetic deletion of 8b in a live virus resulted in increased IFN-I expression (2). Both this manuscript and that of Wong et. al demonstrated that innate immune antagonism is nuanced in CoVs, as differences in cell type, organ tropism, or virus strain utilized can provide different results. Overexpression assays alone are insufficient to capture these differences (summarized in Table 1). Here, we show that JHMV I protein functions as an innate immune antagonist with mRNA levels of multiple IFN-I, cytokines, and chemokines significantly elevated or remaining equivalent between the two viruses despite significant reduction in rJHMV^{IΔ57-137} titers (Fig. 2A; Fig. 1D). These data are similar to those obtained in mice infected with SARS-CoV-2 9b KO virus, which displayed increased mRNA levels of IFN-I but similar levels of cytokines and chemokines in the lungs compared with mice infected with rSARS-CoV-2 despite significant attenuation (6). The immunoevasive properties of SARS-CoV-2 9b protein have largely been linked to interactions with mitochondrial proteins including TOM70 and NEMO and downstream IFN-I molecules such as the MAVS/TRAF3/TRAF6 signalosome (3, 5, 6, 27). These papers evaluated mitochondrial damage and reduction in IFN-I levels only in the context of ORF9b overexpression and colocalization of ORF9b or ORF8b with TOM70 or other adaptor molecules. However, these interactions have not been verified in an infectious virus infection to our knowledge. We performed confocal microscopy to evaluate colocalization of JHMV and A59 I with TOM70 and found no significant colocalization between these proteins, recognizing however, that MHV I proteins do not contain the mitochondrial transit peptide predicted for 9b and 8b (Fig. 8C). Interestingly, all live virus colocalization studies have shown I protein cellular localization with the Golgi, which coincides with CoV structural protein localization and virion assembly (Fig. 8A; Table 1). It remains to be determined what specific aspect of the IFN-I signaling pathway is disrupted by rJHMV I, but our analysis indicates it may be independent of the mitochondria-IFN-I interface.

Overall, our data indicate that CoV internal N genes share many unique functions but also evolve in a strain-dependent manner to optimize viral replication. The JHMV I protein aids in modest innate immune antagonism but, importantly, is required for the maintenance of maximal virion infectivity. Loss of the JHMV I protein disrupts virion assembly, which ultimately results in a highly attenuated virus, demonstrated *in vitro* and *in vivo*. Additional studies will be required to identify the precise mechanism by which the I protein aids in CoV assembly.

Limitations

This study has some limitations. It would have benefited from the use of an anti-JHMV I antibody, but such an antibody is not available commercially. We did not develop an anti-JHMV I antibody because, unlike A59 I protein for which an antibody is available,

TABLE 1 Internal N gene function and localization

Virus	Function in infectious	Function in overexpression	Organelle localization		Virion	Ref
	virus		Infectious virus	Overexpression	localization	
JHMV I	Immunoevasive (IFN-I, chemokines), virion structural protein	Unknown	Golgi/ERGIC	Unknown	Yes	This study
A59 I	Mild immunoevasive, virion structural protein	Unknown	Golgi/ERGIC	Unknown	Yes	This study and (1)
MERS 8b	Potent IFN-I antagonist	IFN-I antagonist, inhibits upstream IRF3	Golgi/ER	Mitochondria (TOM70)	Unknown	(2, 6, 26)
SARS 9b	Virion structural protein	Immunoevasive (IFN-I, chemokines)	Unknown	Mitochondria (DRP1/MAVS)	Yes	(3, 7)
SARS2 9b	Immunoevasive (IFN-I)	IFN-I antagonist at mitochondria/TOM70 interface and NFκB antagonist targeting NEMO	Unknown	Mitochondria (TOM70)	Unknown	(4–6, 22, 27)

September 2024 Volume 98 Issue 9 10.1128/jvi.00680-24**16**

JHMV I lacks a N terminal hydrophilic domain and is highly hydrophobic. The A59 I-specific antibody recognized the hydrophilic N terminal domain. Similarly, MERS-CoV 8b protein has an N terminal hydrophilic domain and this domain was the target of the MERS-CoV I antibody. The SARS-CoV-2 9b protein lacks a N terminal hydrophilic domain and is hydrophobic. We tried unsuccessfully to generate a SARS-CoV-2 9b antibody. Given the parallels between A59 I/JHMV I and MERS-CoV 8b/SARS-CoV-2 9b, we felt that developing an antibody to JHMV I protein would not be fruitful. Consequently, as described herein, we utilized a V5-tagged I protein inserted into ORF4 of rJHMV to detect the presence of JHMV I in cells and virions.

MATERIALS AND METHODS

Mice

Five- to seven-week-old pathogen-free C57BL/6 and IFNAR^{-/-} mice were purchased from Charles River Laboratories/NCI.

Cells, viruses, and plasmids

17Cl-1 mouse fibroblast cells, HeLa cells expressing the MHV receptor carcinoembryonic antigen-related cell adhesion molecule 1 (HeLa-MHVR), BHK-21 cells, and 293T cells were grown in Dulbecco's modified Eagle medium (DMEM) supplemented with 10% fetal bovine serum, 100 U/mL penicillin and streptomycin, L-glutamine, sodium pyruvate, HEPES, and non-essential amino acids and maintained at 37°C. BMDMs were harvested from C57BL/6 WT and IFNAR-/- mice and differentiated in DMEM media supplemented with 10% FBS, 10% L929 cell supernatant (to supply GM-CSF), 100 U/mL penicillin and streptomycin, L-glutamine, and sodium pyruvate. BMDM cell media were changed daily following the fourth day of differentiation, and cells were infected on the seventh or eighth day post collection.

Recombinant rJHMV and rJHMV $^{\text{Id57-137}}$ were generated as described below. rA59 and rA59 $^{\text{I-KO}}$ were kindly provided by Paul Masters. All viruses were passaged and propagated on 17Cl-1s and titered on HeLa-MVR. IFN-beta, NFkB, and ISRE luciferase reporters, and pCAGs vector were obtained as previously described (28).

Generation of rJHMV^{I∆57-137}

rJHMV^{IΔ57-137} viruses were generated using lambda red recombination with I-Scel homing endonuclease as previously described (29). In brief, forward and reverse primers containing sequences complementary to the I gene of rJHMV, including two stop codons L56* and L73*, followed by a sequence complementary to the target plasmid (pEP-KanS) were designed. These primers were used to amplify the pEP-KanS fragment with overlapping ends carrying rJHMV sequences. PCR fragments were purified using a PureLink Quick Gel Extraction and PCR Purification Combo Kit (Invitrogen). Purified pEP-KanS PCR fragments were electroporated into the GS1783 strain of *Escherichia coli* carrying the rJHMV BAC. Successful recombinants were selected with kanamycin resistance, and the kanamycin markers were later removed via arabinose induction of I-Scel cleavage followed by homologous recombination of the overlapping ends. Successful recombinants were selected by replica plating for the loss of kanamycin resistance and sequence prior to transfection.

Of note, the I protein is only partly deleted in rJHMV $^{\text{Id57-137}}$ unlike in rA59 $^{\text{I-KO}}$. rJHMV $^{\text{Id57-137}}$ was designed similarly to our previously described MERS-CoV 8b KO and SARS-CoV-2 9b KO viruses. We added two stop codons to abrogate expression of the internal N protein without affecting N protein sequence. We were unable to place a N gene-silent stop codon further upstream in the JHMV recombinants. It is possible that an N terminal fragment of the I gene is translated, but we lack the antibody to detect it at present.

The primer sequences used for the $rJHMV^{l\Delta57-137}$ mutant are as follows (stop codons bolded):

Forward: 5'- GATATCGAAGGAGTAGTCTGGGTCGCAAGCCAACAGGCCGAGACTAGGACCT CTGCCGATATTGTAGAAAGGGACCCAAGAGGATGACGACGATAAGTAG-3'

Reverse: 5'- CCTGAGCCTTCAACATAAAAACCTTGAGGCAATACCGTACCGGGCGCAAACCT AGTAGGAATAGCCTCATGGCTACAACCAATTAACCAATTCTGATTAG-3'.

Generation of recombinant MHV I-tagged viruses and plasmids

For JHMV- and A59 I V5-tagged plasmids, JHMV I or A59 I was amplified from purified viral DNA with primers containing cleavage sites for insertion into the pCAGs vector and the V5 tag at the C-terminus. PCR fragments were purified as described above. JHMV I and A59 I were inserted into pCAGs, which was linearized with Xbal and Notl. pCAGs plasmids containing I genes were transfected into 293T cells to verify V5 tag expression. V5-tagged I genes were amplified from pCAGs plasmid with primers overlapping rJHMV ORF4 as previously described (30, 31). A two-step linear recombination process was used to insert the genes of interest (30). The first step removed and replaced the ORF4 sequence with GalK-Kan selection marker while the second step removed and replaced the GalK-Kan selection marker with the PCR-amplified V5-tagged I inserts from the pCAGs plasmid. In brief, the GalK-Kan selection marker was PCR amplified from pYD-C225 (31) and gel purified. Gel-purified GalK-Kan fragments were transformed into SW102 cells carrying the rJHMV BAC by electroporation and linear lambda red recombination. Successful recombinants were selected by Kanamycin resistance culture plates. Verified recombinants carrying the GalK-Kan cassette were replaced with the corresponding rJHMV I- and A59 V5-tagged I inserts by electroporation and a second round of linear lambda red recombination. Successful recombinants were selected using 2-deoxy-galactose-based culture plates, and sequence identity was verified by Sanger sequencing. GalK-Kan selection markers were amplified with the following primers:

Insertion of GalK cassette into MHV ORF4

Forward 5'-CTCTCCTGGAAAGACAGAAATCTAAACAATTTATAGCATTCTCATTGCTACTTT GCTCCTCTAGAGGGCAGCAAGTAGTTcctgttgacaattaatcatcg-3'

Capital letters represent sequence flanking the area of interest in the rJHMV BAC; sequences complementary to pYD-C225 are shown as lowercase letters.

MHV I with ORF4 overlap primers (ORF4 nucleotides in lowercase and MHV nucleotides in uppercase):

rJHMV I V5 Forward:

 $5'\mbox{-}tag cattet cattget actttget cetetag aggge agea agt agt tATGGAATCCCAGCTTCACAGCAGCAGAA-3'$

rA59 I V5 Forward:

5'-tagcattctcattgctactttgctcctctagagggcagcaagtagttATGGAATCCTCAAGAAGAC-CACTT-3' MHV I V5 Reverse for both JHMV and A59 I: 5'-ggacggc-cagaattaagatgaggtttagaactagtaatataatctagagtTTACGTAGAATCGAGACCGAGGAGA-3'

Rescue of BAC-derived virus

Two micrograms of the rJHMV $^{\text{I}\Delta57-137}$ BAC and 1 μ g MHV N plasmid were transfected into BHK-21 cells with Lipofectamine 3000 (Invitrogen) in a six-well plate according to the manufacturer's protocol. Cultures were harvested at 2–3 dpi when CPE had formed. Viruses were then propagated on 17Cl-1 cells as described, and the I gene was sequenced to confirm mutations.

Tissue culture cell infection

Virus stocks were created by infecting 17Cl-1 cells at an MOI of 0.01 PFU/cell and collecting both the cells and supernatant at 16–20 hpi. The cells were freeze thawed,

and debris was removed via centrifugation prior to collecting virus stocks. Virus stocks were quantified by plaque assay on Hela-MHVR cells. BMDM cells were infected with MHV at the indicated MOI. For rA59 plaque assays, agarose overlays were fixed with 3.7% formaldehyde at 16 to 24 hpi and stained with 0.1% crystal violet. For rJHMV plaque assays, agarose overlay with 1% neutral red was overlaid after 16 hpi and plaques were counted at 20 hpi.

Mouse infections

Five- to seven-week-old male C57BL/6 or IFNAR^{-/-} mice were anesthetized with isoflurane and inoculated intranasally with 12 μ L of rJHMV at 60,000 PFU or 20,000 PFU, respectively. Clinical scoring for rJHMV infection was based on the following criteria: 0, asymptomatic; 1, limp tail, mild hunching; 2, wobbly gait with mild righting difficulty, hunching; 3, hind limb paresis and extreme righting difficulty; 4, hind limb paralysis; and 5, moribund. Five- to seven-week-old male C57BL/6 mice were anesthetized with ketamine/xylazine and intracranially inoculated with 30 μ L A59 at 30,000 PFU or intrahepatically with 10,000 PFU/300 μ L. All mice were weighed and monitored daily for 2 weeks. Animals were humanely euthanized if weights dropped below 70% of the initial weight or were moribund in accordance with animal protocol.

Flow cytometry

Mice were sacrificed and perfused with phosphate-buffered saline (PBS) at indicated dpi. Brains were harvested and processed using an adult mouse brain isolation kit (Miltenyi) and dissociated on the Octomax (Miltenyi) per the manufacturer's instructions. Pelleted cells were then washed and resuspend in FC block with Live/Dead blue stain (Invitrogen) followed by surface stain antibodies for flow cytometry on the Cytek Aurora. The following antibodies were used for flow cytometry in this study: BV570 α -CD45 (30-F11; BioLegend), eFluor 450 α -CD11b (M1/70; eBioscience), PerCP α -Ly6G (1A8 BioLegend), APC/eFluor 780 α -Ly6C (HK1.4; Invitrogen), MHC-II BV605 (M5/114.15.2 BioLegend), and BV750 α -CD3 (17A2 BioLegend).

RNA isolation and gRT-PCR

RNA was isolated from cells using TRIzol (Thermo Fisher Scientific) and PureLink RNA Mini Kit (Thermo Fisher Scientific) as per the manufacturer's instructions. cDNA was prepared using MMLV-reverse transcriptase as per the manufacturer's instructions (Thermo Fisher Scientific). Quantitative PCR (qPCR) was performed on a QuantStudio3 real-time PCR system using PowerUp SYBR Green Master Mix (Thermo Fisher Scientific). Mouse qPCR primers were used as previously described (32). Cycle thresholds were normalized to that of housekeeping gene hypoxanthine-guanine phosphoribosyltransferase (HPRT) by the following equation: Δ CT = CT (gene of interest)—CT (HPRT). All results are shown as a ratio to HPRT/GAPDH calculated as -2Δ CT.

Co-IP and western blotting

For Co-IP, infected monolayer 17Cl-1 cells were lysed with IP buffer [0.5% NP-40, 150 mM NaCl, 5% glycerol, and 50 mM Tris (pH 8.0)], containing a protease inhibitor cocktail (Thermo 106 Fisher Scientific). Supernatants were collected, and debris was removed by centrifugation. Cell lysates were applied to protein G Dynabeads (Thermo Fischer Scientific) conjugated to Anti-V5tag antibody at 4°C overnight. Lysates were washed three times and boiled in 1× Laemmli sample buffer. Alternatively, virions and cells were lysed in 1× Laemmli buffer. All proteins were separated by SDS-PAGE and were transferred to polyvinylidene difluoride membranes (Millipore). Membranes were blocked with 5% milk in 1× Tris-buffered saline, 0.1% Tween 20 detergent (TBST). Blots were incubated with listed primary antibodies overnight at 4°C. Rabbit anti-JHM32 (1:10,000) (Perlman Lab), anti-V5 (1:1,000), anti-actin (1:5,000) (Invitrogen 15G5A11/E2),

and secondary HRP-conjugated anti-rabbit (Invitrogen 31458) or anti-mouse (Amersham NA931VS) (1:5,000) antibodies were applied at room temperature for 1.5 hours.

Virion purification

17Cl-1 cells were infected at an MOI of 0.01, and cells and supernatants were collected via freeze thawing at 16 hpi. Samples were clarified at 1,300 RPM for 5 min and then 4,000 RPM for 10 min to pellet cellular debris and then filtered through a 45-mm filter. Filtered supernatant was underlaid with 20% iodixanol and centrifuged at 10,000 RPM on an SW28 Rotor for 24 hours at 4°C to concentrate virions. Concentrated virions were applied to a 10%/40% iodixanol step gradient, which was then centrifuged at 35,000k on a Beckman SW41 Rotor for 1 hour at 4°C. Ten fractions were removed for titers and protein expression via plaque assay and western blot, respectively.

RNA to PFU ratio

BMDM cells were infected at an MOI of 0.01 with the rJHMV and rJHMV^{IA57-137}. Cells and supernatants were collected separately at 12 hpi. Half was used for viral titer by plaque assay, and the other half used for RNA isolation and qRT-PCR for gRNA as previously described (33).

Immunofluorescent microscopy

Sub-confluent monolayers of 17Cl-1 cells were seeded on glass coverslips coated with poly(L)lysine and infected with rJHMV^{JHM-I} or rJHMV^{A59-I} at an MOI of 0.1. At 8 hpi, monolayers were fixed with 4% paraformaldehyde and permeabilized/blocked with 0.1% Triton X-100 in PBS containing 1% goat serum. Cells were stained with the indicated primary antibodies [α-V5, Invitrogen Cat. # R960-25; α-TOM70, Abcam Cat.# ab289977, GM-130(Golgi) Cell Signaling #12480, α-Calnexin (ER) Abcam, ab22595] overnight at 4°C, at 1:100 dilution. Cells were washed before mounting with Vectashield antifade reagent containing DAPI (Vector Laboratories). Pearson's correlation coefficients were obtained by analyzing eight images with an average of three infected cells using Fiji's Manders Coefficient plugin.

Electron microscopy

Samples were post-fixed with 1% osmium tetroxide solution, treated with 2.5% uranyl acetate, dehydrated, and embedded in Epon resin. After overnight polymerization in an oven at +60°C, sections were cut on the Leica EM UC7 ultramicrotome to 80-nm thickness and mounted on copper slot grids for use in transmission electron microscopy. These sections were contrasted with 5% uranyl acetate and Reynolds lead citrate and imaged on a Hitachi HT7800 transmission electron microscope. Viruses were identified based on parameters outlined previously (25). JHMV-infected macrophages form syncytia, with 5–15 nuclei/syncytia. Therefore, for quantification of virions, we imaged nuclei from 5 to 10 cells. Virions per field were quantified blindly.

Sequence alignment and structural predictions

Whole genome sequences belonging to MHV-A59 (NC_048217), MHV-JHM (FJ647226), MHV-1 (FJ647223), MHV-2 (AF201929), and MHV-3 (FJ647224) were acquired from NCBI GenBank (https://www.ncbi.nlm.nih.gov/genbank/). The internal protein sequences found in MERS-CoV (NC_019843), SARS-CoV (NC_004718), and SARS-CoV-2 (NC_045512) were acquired from NCBI Protein (https://www.ncbi.nlm.nih.gov/protein/). For well-annotated genomes, the genes encoding for the I protein were manually obtained. To identify putative I genes from lesser annotated genomes (i.e., MHV-2 and MHV-3), nucleocapsid genes were aligned using Clustal Omega (34). These putative I genes were extracted and then translated using the Expasy Translation Tool (https://web.expasy.org/translate/). Protein sequences were aligned using MUSCLE on MEGA (v11.0.13) (35, 36). Align-

ments (both nucleotide and protein) were visualized with MView (https://www.ebi.ac.uk/jdispatcher/msa/mview) (37).

The structures for both I proteins in MHV-JHM and MHV-A59 were predicted using AlphaFold2 with MMSeq2 (ColabFold v1.5.5) (38). Default modeling settings were maintained throughout. For each protein, five individually top-ranked models were downloaded, along with their respective quality assessment metrics: the multiple sequence alignment coverage, predicted aligned error, and predicted local distance difference tests across residues. Models were then examined, and images were acquired using UCSF Chimera (v1.17.3) (39).

Statistical analysis

An unpaired two-tailed Student's t-test was used to assess differences in means between groups, and graphs are expressed as mean SEM. The n value represents the number of biologic replicates including in a singular independent experiment unless otherwise noted. P values are denoted with P = 0.05, P = 0.01, P = 0.001, and P = 0.001.

ACKNOWLEDGMENTS

We thank the members of the Drs. Stanley Perlman, Wendy Maury, and Richard Roller laboratories for valuable discussions. We thank Dr. Paul Masters for providing A59 and A59^{I-KO} viruses and the A59 I antibody. We thank the University of Iowa Central Microscopy Research Facility for training on confocal microscopy and performing electron microscopy. We acknowledge the Flow Cytometry Facility within the Carver College of Medicine for training and use of flow cytometric equipment.

This work was supported in part by grants from the NIH (R01 NS36592, S.P.; R00 AI170996, L-.Y.R.W.; and T32AI007533, S.A.L.).

AUTHOR AFFILIATIONS

¹Department of Microbiology and Immunology, University of Iowa, Iowa City, Iowa, USA ²Department of Pediatrics, University of Iowa, Iowa City, Iowa, USA

PRESENT ADDRESS

Lok-Yin Roy Wong, Department of Microbiology, Biochemistry and Molecular Genetics, Rutgers University, New Jersey Medical School, Newark, New Jersey, USA Abby Odle, Department of Microbiology, Biochemistry and Molecular Genetics, Rutgers University, New Jersey Medical School, Newark, New Jersey, USA

AUTHOR ORCIDs

Shea A. Lowery http://orcid.org/0000-0002-1652-324X Lok-Yin Roy Wong http://orcid.org/0000-0002-0727-8289 Stanley Perlman http://orcid.org/0000-0003-4213-2354

FUNDING

Funder	Grant(s)	Author(s)
HHS NIH National Institute of Allergy and Infectious Diseases (NIAID)	R01NS36592	Stanley Perlman
HHS NIH National Institute of Allergy and Infectious Diseases (NIAID)	R00Al170996	Lok-Yin Roy Wong
HHS NIH National Institute of Allergy and Infectious Diseases (NIAID)	T32Al007533	Shea A. Lowery

AUTHOR CONTRIBUTIONS

Shea A. Lowery, Conceptualization, Data curation, Formal analysis, Investigation, Methodology, Resources, Supervision, Validation, Visualization, Writing – original draft, Writing – review and editing | Noah Schuster, Data curation, Investigation | Lok-Yin Roy Wong, Conceptualization, Investigation | Thomas Carrillo Jr., Investigation | Erin Peters, Investigation | Abby Odle, Investigation | Alan Sariol, Investigation | Isabella Cesarz, Data curation, Investigation | Pengfei Li, Data curation, Investigation | Stanley Perlman, Conceptualization, Data curation, Formal analysis, Funding acquisition, Investigation, Methodology, Project administration, Resources, Supervision, Validation, Visualization, Writing – original draft, Writing – review and editing

DATA AVAILABILITY

All data are shown in the paper and are further available upon request.

ETHICS APPROVAL

All animal studies were approved by the University of Iowa IACUC under protocol #9051795-043.

ADDITIONAL FILES

The following material is available online.

Supplemental Material

Figure S1 (JVI00680-24-s0001.tiff). Sequence and structural predictions of JHMV and A59 I

Figure S2 (JVI00680-24-s0002.tiff). Characterization of rJHMV^{IΔ57-137}.

REFERENCES

- Fischer F, Peng D, Hingley ST, Weiss SR, Masters PS. 1997. The internal open reading frame within the nucleocapsid gene of mouse hepatitis virus encodes a structural protein that is not essential for viral replication. J Virol 71:996–1003. https://doi.org/10.1128/JVI.71.2.996-1003.1997
- Wong L-Y, Ye Z-W, Lui P-Y, Zheng X, Yuan S, Zhu L, Fung S-Y, Yuen K-S, Siu K-L, Yeung M-L, Cai Z, Woo P-Y, Yuen K-Y, Chan C-P, Jin D-Y. 2020. Middle east respiratory syndrome coronavirus ORF8b accessory protein suppresses type I IFN expression by impeding HSP70-dependent activation of IRF3 kinase IKKE. J Immunol 205:1564–1579. https://doi.org/10.4049/jimmunol.1901489
- Shi C-S, Qi H-Y, Boularan C, Huang N-N, Abu-Asab M, Shelhamer JH, Kehrl JH. 2014. SARS-coronavirus open reading frame-9b suppresses innate immunity by targeting mitochondria and the MAVS/TRAF3/TRAF6 signalosome. J Immunol 193:3080–3089. https://doi.org/10.4049/ jimmunol.1303196
- Lenhard S, Gerlich S, Khan A, Rödl S, Bökenkamp J-E, Peker E, Zarges C, Faust J, Storchova Z, Räschle M, Riemer J, Herrmann JM. 2023. The Orf9b protein of SARS-CoV-2 modulates mitochondrial protein biogenesis. J Cell Biol 222:e202303002. https://doi.org/10.1083/jcb.202303002
- Jiang H-W, Zhang H-N, Meng Q-F, Xie J, Li Y, Chen H, Zheng Y-X, Wang X-N, Qi H, Zhang J, Wang P-H, Han Z-G, Tao S-C. 2020. SARS-CoV-2 Orf9b suppresses type I interferon responses by targeting TOM70. Cell Mol Immunol 17:998–1000. https://doi.org/10.1038/s41423-020-0514-8
- Wong L-YR, Odle A, Luhmann E, Wu DC, Wang Y, Teo QW, Ptak C, Sariol A, Lowery S, Mack M, Meyerholz DK, Wu NC, Radoshevich L, Perlman S. 2023. Contrasting roles of MERS-CoV and SARS-CoV-2 internal proteins in pathogenesis in mice. mBio 14:e0247623. https://doi.org/10.1128/ mbio.02476-23
- Xu K, Zheng B-J, Zeng R, Lu W, Lin Y-P, Xue L, Li L, Yang L-L, Xu C, Dai J, Wang F, Li Q, Dong Q-X, Yang R-F, Wu J-R, Sun B. 2009. Severe acute respiratory syndrome coronavirus accessory protein 9b is a

- virion-associated protein. Virology 388:279–285. https://doi.org/10.1016/j.virol.2009.03.032
- Shen S, Lin P-S, Chao Y-C, Zhang A, Yang X, Lim SG, Hong W, Tan Y-J. 2005. The severe acute respiratory syndrome coronavirus 3a is a novel structural protein. Biochem Biophys Res Commun 330:286–292. https:// doi.org/10.1016/j.bbrc.2005.02.153
- Huang C, Ito N, Tseng C-TK, Makino S. 2006. Severe acute respiratory syndrome coronavirus 7a accessory protein is a viral structural protein. J Virol 80:7287–7294. https://doi.org/10.1128/JVI.00414-06
- Huang C, Peters CJ, Makino S. 2007. Severe acute respiratory syndrome coronavirus accessory protein 6 is a virion-associated protein and is released from 6 protein-expressing cells. J Virol 81:5423–5426. https:// doi.org/10.1128/JVI.02307-06
- Ito N, Mossel EC, Narayanan K, Popov VL, Huang C, Inoue T, Peters CJ, Makino S. 2005. Severe acute respiratory syndrome coronavirus 3a protein is a viral structural protein. J Virol 79:3182–3186. https://doi.org/ 10.1128/JVI.79.5.3182-3186.2005
- Schaecher SR, Mackenzie JM, Pekosz A. 2007. The ORF7b protein of severe acute respiratory syndrome coronavirus (SARS-CoV) is expressed in virus-infected cells and incorporated into SARS-CoV particles. J Virol 81:718–731. https://doi.org/10.1128/JVI.01691-06
- Dediego ML, Pewe L, Alvarez E, Rejas MT, Perlman S, Enjuanes L. 2008. Pathogenicity of severe acute respiratory coronavirus deletion mutants in hACE-2 transgenic mice. Virology 376:379–389. https://doi.org/10. 1016/j.virol.2008.03.005
- Knobler RL, Haspel MV, Oldstone MB. 1981. Mouse hepatitis virus type 4 (JHM strains). Induced fatal central nervous system disease. I. Genetic control and murine neuron as the susceptible site of disease. J Exp Med 153:832–843. https://doi.org/10.1084/jem.153.4.832
- Fleming JO, Trousdale MD, el-Zaatari FA, Stohlman SA, Weiner LP. 1986.
 Pathogenicity of antigenic variants of murine coronavirus JHM selected

- with monoclonal antibodies. J Virol 58:869–875. https://doi.org/10.1128/JVI.58.3.869-875.1986
- Perlman S, Wheeler DL. 2016. Neurotropic coronavirus infections. Neurotrop Viral Infect:115–148. https://doi.org/10.1007/978-3-319-33133-1
- Ontiveros E, Kuo L, Masters PS, Perlman S. 2001. Inactivation of expression of gene 4 of mouse hepatitis virus strain JHM does not affect virulence in the murine CNS. Virology 289:230–238. https://doi.org/10. 1006/viro.2001.1167
- Klumperman J, Locker JK, Meijer A, Horzinek MC, Geuze HJ, Rottier PJ. 1994. Coronavirus M proteins accumulate in the Golgi complex beyond the site of virion budding. J Virol 68:6523–6534. https://doi.org/10.1128/ JVI.68.10.6523-6534.1994
- Tooze J, Tooze S, Warren G. 1984. Replication of coronavirus MHV-A59 in sac- cells: determination of the first site of budding of progeny virions. Eur J Cell Biol 33:281–293.
- Liu DX, Fung TS, Chong KK-L, Shukla A, Hilgenfeld R. 2014. Accessory proteins of SARS-CoV and other coronaviruses. Antiviral Res 109:97–109. https://doi.org/10.1016/j.antiviral.2014.06.013
- Krijnse-Locker J, Ericsson M, Rottier PJ, Griffiths G. 1994. Characterization
 of the budding compartment of mouse hepatitis virus: evidence that
 transport from the RER to the Golgi complex requires only one vesicular
 transport step. J Cell Biol 124:55–70. https://doi.org/10.1083/jcb.124.1.55
- Gao X, Zhu K, Qin B, Olieric V, Wang M, Cui S. 2021. Crystal structure of SARS-CoV-2 Orf9b in complex with human TOM70 suggests unusual virus-host interactions. Nat Commun 12:2843. https://doi.org/10.1038/ s41467-021-23118-8
- Navas-Martin S, Brom M, Chua M-M, Watson R, Qiu Z, Weiss SR. 2007. Replicase genes of murine coronavirus strains A59 and JHM are interchangeable: differences in pathogenesis map to the 3' one-third of the genome. J Virol 81:1022–1026. https://doi.org/10.1128/JVI.01944-06
- Machamer CE. 2013. Accommodation of large cargo within golgi cisternae. Histochem Cell Biol 140:261–269. https://doi.org/10.1007/ s00418-013-1120-y
- Bullock HA, Goldsmith CS, Miller SE. 2021. Best practices for correctly identifying coronavirus by transmission electron microscopy. Kidney Int 99:824–827. https://doi.org/10.1016/j.kint.2021.01.004
- Li Y, Jin Y, Kuang L, Luo Z, Li F, Sun J, Zhu A, Zhuang Z, Wang Y, Wen L, Liu D, Chen C, Gan M, Zhao J, Zhao J. 2022. The N-terminal region of middle east respiratory syndrome coronavirus accessory protein 8b Is essential for enhanced virulence of an attenuated murine coronavirus. J Virol 96:e0184221. https://doi.org/10.1128/JVI.01842-21
- Wu J, Shi Y, Pan X, Wu S, Hou R, Zhang Y, Zhong T, Tang H, Du W, Wang L, Wo J, Mu J, Qiu Y, Yang K, Zhang L-K, Ye B-C, Qi N. 2021. SARS-CoV-2 ORF9b inhibits RIG-I-MAVS antiviral signaling by interrupting K63-linked

- ubiquitination of NEMO. Cell Rep 34:108761. https://doi.org/10.1016/j.celrep.2021.108761
- Zhou H, Perlman S. 2007. Mouse hepatitis virus does not induce Beta interferon synthesis and does not inhibit its induction by doublestranded RNA. J Virol 81:568–574. https://doi.org/10.1128/JVI.01512-06
- Fehr AR. 2020. Bacterial Artificial Chromosome-Based Lambda Red Recombination with the I-Scel Homing Endonuclease for Genetic Alteration of MERS-CoV, p 53–68. In Vijay R (ed), MERS Coronavirus: Methods and Protocols Methods in Molecular Biology. Vol. 2099.
- Warming S, Costantino N, Court DL, Jenkins NA, Copeland NG. 2005.
 Simple and highly efficient BAC recombineering using galK selection.
 Nucleic Acids Res 33:e36. https://doi.org/10.1093/nar/gni035
- Fehr AR, Yu D. 2010. Human cytomegalovirus gene UL21a encodes a short-lived cytoplasmic protein and facilitates virus replication in fibroblasts. J Virol 84:291–302. https://doi.org/10.1128/JVI.01116-09
- Zhou H, Zhao J, Perlman S. 2010. Autocrine interferon priming in macrophages but not dendritic cells results in enhanced cytokine and chemokine production after coronavirus infection. mBio 1:e00219-10. https://doi.org/10.1128/mBio.00219-10
- Case JB, Li Y, Elliott R, Lu X, Graepel KW, Sexton NR, Smith EC, Weiss SR, Denison MR. 2018. Murine hepatitis virus nsp14 exoribonuclease activity is required for resistance to innate immunity. J Virol 92:e01531-17. https://doi.org/10.1128/JVI.01531-17
- Sievers F, Wilm A, Dineen D, Gibson TJ, Karplus K, Li W, Lopez R, McWilliam H, Remmert M, Söding J, Thompson JD, Higgins DG. 2011. Fast, scalable generation of high-quality protein multiple sequence alignments using clustal omega. Mol Syst Biol 7:539. https://doi.org/10. 1038/msb.2011.75
- Edgar RC. 2004. MUSCLE: multiple sequence alignment with high accuracy and high throughput. Nucleic Acids Res 32:1792–1797. https:// doi.org/10.1093/nar/gkh340
- Tamura K, Stecher G, Kumar S. 2021. MEGA11: molecular evolutionary genetics analysis version 11. Mol Biol Evol 38:3022–3027. https://doi.org/ 10.1093/molbev/msab120
- Brown NP, Leroy C, Sander C. 1998. MView: a web-compatible database search or multiple alignment viewer. Bioinformatics 14:380–381. https://doi.org/10.1093/bioinformatics/14.4.380
- Mirdita M, Schütze K, Moriwaki Y, Heo L, Ovchinnikov S, Steinegger M. 2022. ColabFold: making protein folding accessible to all. Nat Methods 19:679–682. https://doi.org/10.1038/s41592-022-01488-1
- Pettersen EF, Goddard TD, Huang CC, Couch GS, Greenblatt DM, Meng EC, Ferrin TE. 2004. UCSF chimera--A visualization system for exploratory research and analysis. J Comput Chem 25:1605–1612. https://doi.org/10. 1002/jcc.20084